HIGH SPEED, WIDE BANDWIDTH SIGNAL DETECTION AND FREQUENCY ESTIMATION

Dr. James R. Caprio
Senior Scientist
Comptek Research
Buffalo, N.Y.

Dr. Lennart Nystrom
Principal Engineer
Anaren Microwave
E. Syracuse, N.Y.

ABSTRACT

A digital frequency discriminator (DFD) of the delay-correlator type is described. The device is shown to have an instantaneous frequency measurement capability on very short pulses. The theoretical performance of the DFD in a noisy background is derived and shown to compare favorably with measured results. Key Words: digital frequency discriminator, delay-correlator, instantaneous frequency measurement.

INTRODUCTION

The digital frequency discriminator is a very high speed, wide-bandwidth microwave device with capability to detect and acquire input pulse frequencies on a monopulse basis. Although its primary application has been in radar warning receivers it can also be utilized in telecommunications as a component of a surveillance receiver for acquisition and analysis of pulsed communications signals in dense pulse environments.

A simplified schematic of the DFD is shown in Figure 1. Input signals are restricted to the RF pass bands $||f|-f_c| \leq W/2$ and the output video band is $|f| \leq B/2$. The lowest input frequency $f_c - W/2$ is also well removed from the video band.

The ratio of output to input SNR will be shown to vary directly with W/B, but a minimum B value is dictated by the requirement for reliable detection and frequency estimation of very narrow pulses. For radar warning applications, for example, pulse widths of 100 nanoseconds must be passed by the video filter. Even in extreme cases, however, W/B can be assumed to be on the order of hundreds.

THEORY OF OPERATION

The input signal is divided between two paths. The upper path inserts a known delay T. Both delayed and undelayed signals are further divided/phase shifted via 90 degree hybrid

couplers. For the frequency range of interest the hybrids may be modeled as perfect Hilbert transformers (with 3dB power loss). Thus, the signals at ports A, B, C, D are:

$$A = [v(t)+\check{v}(t-T)]/2\sqrt{2}, \qquad B = [\check{v}(t)+v(t-T)]/2\sqrt{2}$$

$$C = [v(t)-v(t-T)]/2\sqrt{2}, \qquad D = [\check{v}(t)+\check{v}(t-T)]/2\sqrt{2}$$

where $\check{v}(t)$ denotes the Hilbert transform of v(t) (note: $\check{\check{v}}(t) = -v(t)$). The signal pairs (A,B) and (C,D) are squared by the nonlinear elements and differenced to produce the prefiltered quadrature signals Q(t), I(t). The output quadrature signals are:

$$i(t)= \langle I(t) \rangle , \quad q(t)= \langle Q(t) \rangle$$

where $\langle\ \rangle$ designates the video filtering operation performed by the Ideal Lowpass Filter (ILPF) with transfer function

$$H(f)=1, \quad |f| \le B/2$$

The filtered quadrature signals can be written

$$i(t) = \langle D^2 - C^2 \rangle = \mathrm{Re}\, \langle (D+jC)^2 \rangle , \quad q(t) = \langle B^2 - A^2 \rangle = \mathrm{Re}\, \langle (B+jA)^2 \rangle$$

It will prove convenient to express these in terms of the pre-envelope (analytic signal) a(t) associated with v(t);

$$a(t)=[v(t)+j\check{v}(t)]/2$$

Then one finds

$$i(t) = -\mathrm{Re}\, \langle [a(t)-a^*(t-T)]^2 \rangle /2, \quad q(t) = \mathrm{Re}\, \langle [ja^*(t)+a(t-T)]^2 \rangle /2$$

For convenience, the properties of a(t) are reviewed in the Appendix, where it is shown that a(t) has frequency components only in the band $|f-f_c| \le W/2$ and a*(t) has frequency components only in the negative image band. Squares of these terms will therefore consist of doubled frequencies well outside the video passband. Deleting these yields

$$i(t) = \mathrm{Re}\, \langle a(t)a^*(t-T) \rangle , \quad q(t) = \mathrm{Im}\, \langle a(t)a^*(t-T) \rangle$$

or, combining into a single complex output signal

$$z(t) = i(t)+jq(t) = \langle a(t)a^*(t-T) \rangle \qquad (1)$$

For example, consider a carrier modulated rectangular pulse of amplitude A and duration To;

$$v(t) = A\, p(t) \cos(\omega_o + \theta), \qquad p(t)=1,\ 0 \le t \le To$$

The associated analytic signal is

$$a(t) = \frac{A}{2}\, p(t)\, e^{j(\omega_o t+\theta)}$$

Assuming B is wide enough to pass the pulse undistorted, the complex DFD output is, from (1)

$$z(t) = \frac{A^2}{4} \langle p(t)p(t-T) \rangle\ e^{j\omega_o T} = \frac{A^2}{4} e^{j\omega_o T} \qquad \text{for } T \le t \le To$$

Thus, at any time t in the range (T, To) the pulse frequency and amplitude may be derived from the instantaneous quadrature samples i(t), q(t):

$$f_o = \frac{1}{2\pi T} \tan^{-1}\left[\frac{q(t)}{i(t)}\right], \qquad A = 2\sqrt{i^2(t)+q^2(t)} \tag{2}$$

For further insight to the operation of the DFD, we can approximate the ILPF impulse response h(t) as an integrating window of duration 2D=2/B, i.e.,

$$h(t) = \frac{1}{2D} \qquad -D \le t \le D$$

Then (1) shows

$$z(t) = \int h(t-u)a(u)a^*(u-T)du = \frac{1}{2D}\int_{t-D}^{t+D} a(u)a^*(u-T)du$$

which approaches the time-average autocorrelation of a(t) as D grows. If a(t) is a correlation-ergodic random process, this in turn approaches the statistical (ensemble-average) autocorrelation $Ez(t) = Ea(t)a^*(t-T) = R_{aa}(T)$.

PERFORMANCE IN NOISE

The foregoing example is an idealized illustration that ignores receiver noise effects. The DFD is a wideband device and, as a consequence of the nonlinear (square law) processing, thermal noise throughout the entire band will contribute to the output z(t). For a sinusoidal pulse input the frequency, and amplitude estimates (2) will therefore be noise-corrupted random variables. Here we examine the statistical properties of these estimates by deriving the probability density function of z(t).

Let w(t) denote the receiver input noise. We assume w(t) is a zero-mean, stationary gaussian process with wideband spectrum $S_{ww}(f)$ as illustrated in Figure 2a. A sinusoidal signal $s(t)=A\cos(\omega_o T+\theta)$ arrives causing the total input $v(t)=s(t)+w(t)$. The pre-envelope of v(t) is therefore the complex gaussian process

$$a(t) = \frac{A}{2} e^{j(\omega_o t+\theta)} + n(t) \tag{3}$$

where n(t) is the pre-envelope of w(t). The spectrum $S_{nn}(f)$ is a shifted replica of $S_{ww}(f)$ as shown in Figure 2b. From (1) we find

$$z(t) = \left\langle \frac{A^2}{4} e^{j\omega_o T} + \frac{A}{2} n^*(t-T) e^{j(\omega_o t+\theta)} + \frac{A}{2} n(t) e^{-j(\omega_o t-\omega_o T+\theta)} \right\rangle + \langle n(t)n^*(t-T)\rangle$$

The first bracketed term is clearly gaussian. Representing n(t) as a sum of components $n_i(t)$ having individual spectra $S_{ii}(f)$ (Figure 2c), we observe that since these spectra are non-overlapping, the components are independent gaussian variables. The second term can be expressed as

$$\langle n(t)n^*(t-T)\rangle = \sum_{i,j} \langle n_i(t)n_j^*(t-T)\rangle \approx \sum_i \langle n_i(t)n_i^*(t-T)\rangle$$

since only terms with $i \approx j$ will pass the LPF. Since this sum consists of a very large number (approximately W/B) of independent random variables we can justifiably invoke the Central Limit Theorem to deem it gaussian.

We conclude z(t) is gaussian and to specify its pdf we need only determine its mean and covariance statistics. From the expansion above

$$M = Ez(t) = \frac{A^2}{4} e^{j\omega_o T} + R_{nn}(T) \tag{4}$$

or, in terms of the real quadrature components,

$$M_i = Ei(t) = \frac{A^2}{4} \cos(\omega_o T) + \frac{R_{ww}(T)}{2} \tag{5}$$

$$M_q = Eq(t) = \frac{A^2}{4} \sin(\omega_o T) + \frac{\check{R}_{ww}(T)}{2} \tag{6}$$

are the Re, Im parts of (4). The variances

$$C_{ii} = E[i(t)-M_i]^2 , \quad C_{qq} = E[q(t)-M_q]^2$$

and covariance

$$C_{qi} = E[q(t)-M_q][i(t)-M_q]^2$$

can be derived by application of the properties:

$$En(t)n(t-\tau) = 0 \text{ for all } \tau$$

where n(t) is any analytic process (see Appendix); and

$$Eu_iu_iu_k = 0,$$
$$Eu_1u_2u_3u_4 = Eu_1u_2Eu_3u_4 + Eu_1u_3Eu_2u_4 + Eu_1u_4Eu_2u_3$$

when the u_i are any zero mean gaussian variates. The result is

$$C_{ii} = \frac{1}{2}\int_{-B/2}^{B/2} [C(f,0) + \text{Re } C(f,T)]\, df \tag{7}$$

$$C_{qq} = \frac{1}{2}\int_{-B/2}^{B/2} [C(f,0) - \text{Re } C(f,T)]\, df \tag{8}$$

$$C_{qi} = \frac{1}{2}\int_{-B/2}^{B/2} \text{Im } C(f,T)\ \ df \tag{9}$$

where

$$C(f,T) = \frac{A^2}{4} e^{2j\omega_o T}\left[e^{-j\omega T}\tilde{S}(f_o-f_c-f) + e^{j\omega T}\tilde{S}(f_o-f_c+f)\right] \tag{10}$$

$$+ e^{2j\omega_c T}\int_{-\infty}^{\infty} e^{2j\omega' T}\tilde{S}(f'+f/2)\ \tilde{S}(f'-f/2)\, df'$$

and $\tilde{S}(f)$ is the spectrum of the noise envelope; i.e.,

$$\tilde{S}(f) = S_{nn}(f+f_c) = S_{ww}(f+f_c)U(f+f_c)$$

is the upper sideband of $S_{ww}(f)$ shifted left by f_c (see Figure 2d). We thus have the pdf of the vector z=[i(t) q(t)]', viz.,

$$f(z) = \frac{1}{2\pi\sqrt{|\Lambda|}} \exp\left[-\frac{1}{2}(z-M)^* \Lambda^{-1}(z-M)\right] \tag{11}$$

where (z-M)* is the conjugate transpose of z-M and

$$M = \begin{bmatrix} M_i \\ M_q \end{bmatrix}, \quad \Lambda = \begin{bmatrix} C_{ii} & C_{qi} \\ C_{qi} & C_{qq} \end{bmatrix}, \quad |\Lambda| = C_{ii}C_{qq} - C_{qi}^2$$

The signal frequency and amplitude estimates $\hat{f}_o$, $\hat{A}$ in normalized form are, from (2);

$$\theta = 2\pi \hat{f}_o T = \tan^{-1}\left[\frac{q(t)}{i(t)}\right], \qquad V = \frac{\hat{A}}{2} = \sqrt{i^2(t)+q^2(t)}$$

This transformation has Jacobian equal to V. Applying these to (11) obtains the joint pdf of (θ,V);

$$f(\theta,V) = \frac{V}{2\pi\sqrt{|\Lambda|}} \exp\left\{\frac{-1}{2|\Lambda|}\left[C_{qq}(V\cos\theta - M_i)^2 - 2C_{qi}(V\cos\theta - M_i)(V\sin\theta - M_q) + C_{ii}(V\sin\theta - M_q)^2\right]\right\}$$

$$V \geq 0, \qquad -\pi < \theta \leq \pi$$

We are primarily interested in the accuracy of the frequency estimate

$$\hat{f}_o = \frac{\theta}{2\pi T}$$

hence we integrate f(θ,V) on V to obtain the pdf of θ;

$$f(\theta) = \frac{1}{g_2(\theta)}\sqrt{\frac{|\Lambda|}{2\pi}} \exp\left\{\frac{-g_0}{2|\Lambda|} + \frac{B^2(\theta)}{2}\right\}\left[\frac{1}{\sqrt{2\pi}} \exp\left(-\frac{B^2(\theta)}{2}\right) + B(\theta)\,\mathrm{erf}^*[B(\theta)]\right] \quad 12)$$

where:

$$B(\theta) = \frac{g_1(\theta)}{\sqrt{g_2(\theta)|\Lambda|}}$$

$$g_2(\theta) = C_{qq}\cos^2\theta - 2C_{qi}\sin\theta + C_{ii}\sin^2\theta$$

$$g_1(\theta) = C_{qq}M_i\cos\theta + C_{ii}M_q\sin\theta - C_{qi}(M_q\sin\theta + M_i\sin\theta$$

$$g_0 = C_{qq}M_i^2 - 2C_{qi}M_iM_q + C_{ii}M_q^2$$

and erf*(x) is the gaussian error function:

$$\text{erf*}(x) = \frac{1}{\sqrt{2\pi}} \int_{-\infty}^{x} \exp(-y^2/2)\, dy$$

MEASUREMENT RESULTS

The results above apply for any stationary noise spectrum $S_{ww}(f)$. For ease of comparison with experimental data, however, a relatively flat spectrum

$$\tilde{S}(f) = No/2 \qquad |f| \leq W/2 \tag{13}$$

was generated and signals at various frequencies f_0 were input. Using the special case (13) in equation (10), we find

$$\int_{-B/2}^{B/2} C(f, T)\, df = \left(\frac{NoW}{4}\right)^2 \left[r(1-r/4)\ \text{sinc}\ (BT/2)\text{sinc}(2WT(1-r/4))e^{2j\omega_c T} + 2rP\text{sinc}(BT)e^{2j\omega_o T} \right]$$

where $P=A^2/2NoW$ is the input SNR, and r=B/W is the bandwidth ratio.

To confirm the theoretical performance, an Anaren 2-4.1 GHz band (W = 2.1 GHz) DFD was instrumented for test measurements. Various combinations of SNR (P), video bandwidth (B), delay (T) and signal frequency (f_o) were tested. In all test cases $r << 1$ and $WT >> 1$. Hence, ignoring r/4 and WT terms above and normalizing the overall gain, the predicted gaussian statistics are:

mean:

$$M_i = P\cos(\theta_o) \qquad M_q = P\sin(\theta_o) \tag{14}$$

variance:

$$C_{ii} = \frac{r}{2}[(1+2P)+2sP\cos(2\theta_o)] \qquad C_{qq} = \frac{r}{2}[(1+2P)-2sP\cos(2\theta_o)] \tag{15}$$

covariance:

$$C_{qi} = rsP\sin(2\theta_{o)} \tag{16}$$

where a = sinc(BT) and $\theta_o = \omega_o T$ is the ideal DFD phase.

The variances C_{ii}, C_{qq} were confirmed by selecting f_o in the input band (for each T) such that $\cos(2\theta_o) = 1$. With a CW input signal the measured noise fluctuation power in the I,Q channels should then be

$$C_{ii} = \frac{r}{2}[(1+2P)+2sP], \qquad C_{qq} = \frac{r}{2}[(1+2P)-2sP], \tag{17}$$

The results are summarized below:

T (nsec)	P (dB)	B (MHz)	$\sqrt{C_{ii}}$ (eqn. (17))	$\sqrt{C_{qq}}$ (eqn. (17))	$\sqrt{C_{ii}}$ (measured)	$\sqrt{C_{qq}}$ (measured)
42.55	4.5	4	.107	.035	.117	.032
42.55	4.5	20	.190	.165	.206	.164
42.55	0	4	.068	.032	.079	.031
42.55	0	20	.126	.113	.119	.113
1.92	4.5	20	.242	.069	.200	.064

Overall the theoretical vs. experimental results agree to approximately 10%. This is a fairly reasonable agreement when one considers that aggregate errors in measuring P, B, W and the flat-spectrum approximation (13) may very well be of this order.

A somewhat novel approach was taken to confirm the accuracies of mean values and cross-correlation (C_{qi}) as well as the Central Limit Theorem approximation. The gaussian pdf (11), if valid, has the property that randomly selected samples z will fall outside the ellipse

$$(z-M)^* \Lambda^{-1}(z-M) = C^2$$

with probability $\exp(-C^2/2)$. This ellipse has semi-majpr and semi-minor axes given by

$$L = C\sqrt{\frac{|\Lambda|}{V_{min}}}, \qquad S = C\sqrt{\frac{|\Lambda|}{V_{max}}}$$

where

$$V_{min,max} = \frac{C_{ii}+C_{qq}}{2}\left[1 \quad -/+ \quad \sqrt{1 - \frac{4|\Lambda|}{(C_{ii}+C_{qq})^2}}\right]$$

are the minimum and maximum eigenvalues of the covariance matrix Λ. This ellipse is centered at (M_i,M_q) and the angle of inclination of the major axis (measured counterclockwise from the i(t) axis) is

$$\Psi = \tan^{-1}[(C_{qq}-V_{min})/C_{qi}]$$

Using (15) and (16), one finds the axes length ratio should be

$$\frac{L}{S} = \sqrt{\frac{1+2P(1+|s|)}{1+2P(1-|s|)}} \tag{18}$$

and

$$\Psi = \tan^{-1}\left[\frac{\operatorname{sgn}(s)-\cos 2\theta_o}{\sin 2\theta_o}\right] \begin{array}{l} = \theta_o \text{ if } s > 0 \\ = \theta_o - 90^\circ \text{ if } s < 0 \end{array} \tag{19}$$

Thus, the major axis should point through the origin if s=sinc(BT)>0 and the minor axis should point through the origin if s <0. (If s=0 the ellipse degenerates to a circle and Ψ is meaningless). The axis reversal predicted by (19) is observed in Figure 3 which was obtained by polar display of numerous DFD reads as input frequency was cycled through eight discrete settings. The reasonableness of the axis length ratio (18) is also apparent from the ellipse dimensions.

SUMMARY AND CONCLUSIONS

This paper has described the basic properties of a one channel DFD with gaussian noise input. A general theory has been developed which applies to an arbitrary form of the noise spectrum. The development is an extension of the theory in Ref. [1].

Measurements have been performed with a relatively flat noise spectrum and low input signal to noise ratio. Different video bandwidths and delay times have been tested. As can be seen the agreement between theory and measurements is very good.

The DFD described in this paper is a basic building block in a full-up unit. A typical receiver has 4 of these building blocks with delay times of WT=1,4,16,64. This insures good accuracy and wide bandwidth (usually 3 MHz resolution and 10 GHz bandwidth). To increase the sensitivity and the dynamic range a high gain limiting amplifier precedes the basic building blocks (typically -60 dBm sensitivity and 70 dB dynamic range are thereby achieved). By this approach the sensitivity is determined by amplifier noise rather than the 1/f noise in the detector diodes.

Because the receiver can detect and process the frequency on a monopulse basis the data rate is high (typically 5 MHz). Weak signal suppression within the limiting amplifier provides for more reliable detection with simultaneous signals (the strongest signal is detected and processed).

REFERENCES

[1] Hair, Hugh; 1979; “Performance of Digital Frequency Discriminators (DFD) in Noise”; Anaren Microwave Inc. Internal Report.

ACKNOWLEDGEMENTS

The preceding analysis was performed as a design study for an internal training program at Anaren Microwave with the cooperation of Comptek Research. The authors are indebted to Hugh Hair and Carl Gerst, President, and Vice-President, resp., of Anaren; and to Bill LaSala and Jack Wagner, President and Vice-President, resp., of Comptek for their encouragement of this research. We are especially grateful to Hugh Hair for technical guidance and to our colleagues at Anaren for their valuable comments and help with the measurements.

APPENDIX: BANDPASS PROCESS REPRESENTATIONS

Let w(t) be a real, zero-mean, stationary, bandpass (but wideband) random process with autocorrelation $R_{ww}(\tau)$ and power spectrum $S_{ww}(f)$. The spectrum $S_{ww}(f)$ is an even function of f with sidebands ‘centered’ (not necessarily symmetrically) about a carrier frequency f_c. Figure 2a illustrates a typical spectrum.

The Hilbert transform $\check{w}(t)$ is a time invariant, linear transformation of w(t) described either by the impulse response $h_H(t)=1/(\pi t)$ i.e.

$$\check{w}(t) = \int h_H(t-u)\ w(u)\ du = \frac{1}{\pi}\int \frac{w(u)}{t-u}\ du \qquad \text{(A1)}$$

or the transfer function $H_H(f)=-j\ \mathrm{sgn}(f)$. It follows from (A1) that $\check{w}(t)$ is also real, zero-mean with cross- and auto-correlations given by

$$R_{\check{w}w}(\tau) = E\check{w}(t)w(t-\tau) = \check{R}_{ww}(\tau) = -R_{w\check{w}}(\tau)$$

$$R_{\check{w}\check{w}}(\tau) = E\check{w}(t)\check{w}(t-\tau) = R_{ww}(\tau) \qquad \text{(A2)}$$

Thus, $\check{w}(t)$ and w(t) are jointly stationary. The analytic signal or pre-envelope associated with w(t) is the complex signal

$$n(t) = [w(t)+j\check{w}(t)]/2 \qquad \text{(A3)}$$

From the above definitions it is easy to show that n(t) is a zero-mean, stationary process with autocorrelation

$$R_{nn}(\tau) = En(t)n^*(t-\tau) = [R_{ww}(\tau)+j\check{R}_{ww}(\tau)]/2 \tag{A4}$$

i.e., the analytic signal associated with $R_{ww}(\tau)$. Using (A1)-(A3), one also finds that conjugate complex processes n(t), n*(t) are jointly stationary and uncorrelated, i.e., for all τ;

$$En(t)n(t-\tau) = 0 \tag{A5}$$

The conveyance of analyticity from process n(t) to its autocorrelation $R_{nn}(\tau)$ gives rise to single sideband structure of the spectrum $S_{nn}(f)$. Transforming (A4) and using the Hilbert transfer function, one finds

$$S_{nn}(f) = U(f)\, S_{ww}(f) \tag{A6}$$

where U(f) is the unit-step function, Thus, $S_{nn}(f)$ is a one-sided (upper sideband) spectrum, as illustrated in Figure 2b. This is clearly representative of a carrier modulated signal ñ(t) , i.e.,

$$n(t) = \tilde{n}(t)\, e^{j\omega_c t} \tag{A7}$$

where $\tilde{n}(t)$ is termed the complex envelope associated with w(t). Since

$$\tilde{n}(t) = n(t)\, e^{-j\omega_c t} = [w(t)+j\check{w}(t)]e^{-j\omega_c t/2} \tag{A8}$$

the autocorrelation $R_{\tilde{n}\tilde{n}}(\tau)$ is given by

$$R_{\tilde{n}\tilde{n}}(\tau) = R_{nn}(\tau)\, e^{-j\omega_c\tau} = [R_{ww}(\tau)+j\check{R}_{ww}(\tau)]\, e^{-j\omega_c\tau/2} \tag{A9}$$

comparing (A8), (A9) we see this is the complex envelope associated with $R_{ww}(\tau)$. Transforming (A9) yields the spectrum of the complex envelope;

$$S_{\tilde{n}\tilde{n}}(f) = S_{nn}(f+f_c) = S_{ww}(f+f_c)U(f+f_c) \tag{10}$$

which represents a frequency translation (demodulation) by amount f_c as illustrated in Figure 2d. For processes w(t) strictly bandlimited to $||f|-f_c| \le W/2$, it is apparent that ñ(t) is strictly low-pass bandlimited to $|f| \le W/2$. Properties (A5), (A8) show that the conjugate envelope processes ñ(t),ñ*(t) are also uncorrelated, i.e., for all τ ;

$$E\tilde{n}(t)\tilde{n}(t-\tau) = 0$$

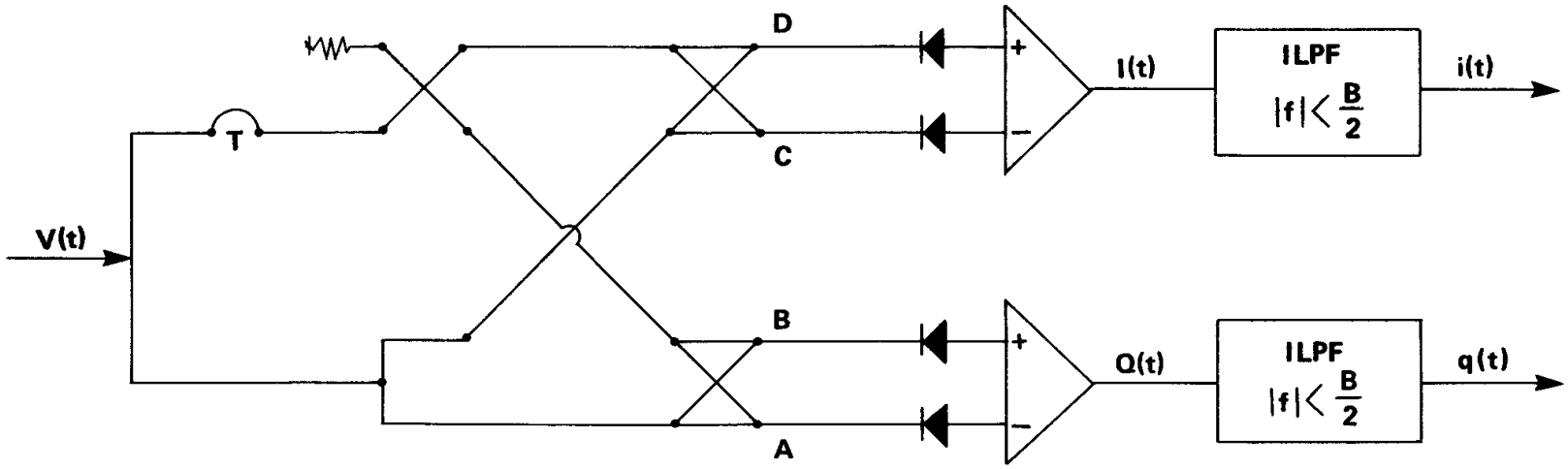

FIGURE 1 DFD Simplified Schematic

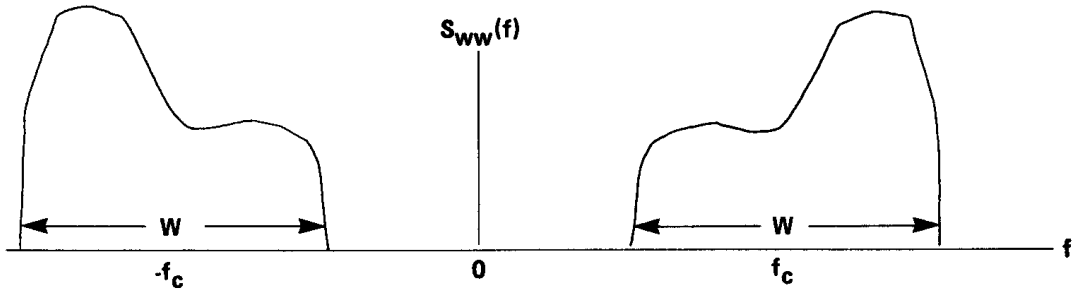

2a. Spectrum of a real, wideband, bandpass process w(t).

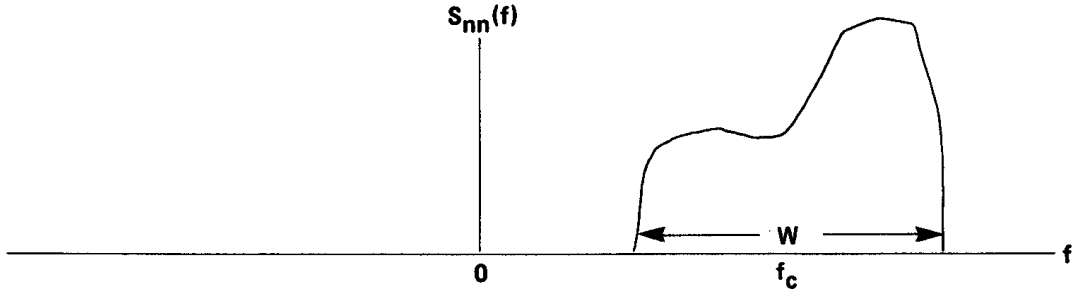

2b. Spectrum of the analytic signal (pre-envelope) $n(t) = \frac{1}{2} [w(t) + j\check{w}(t)]$

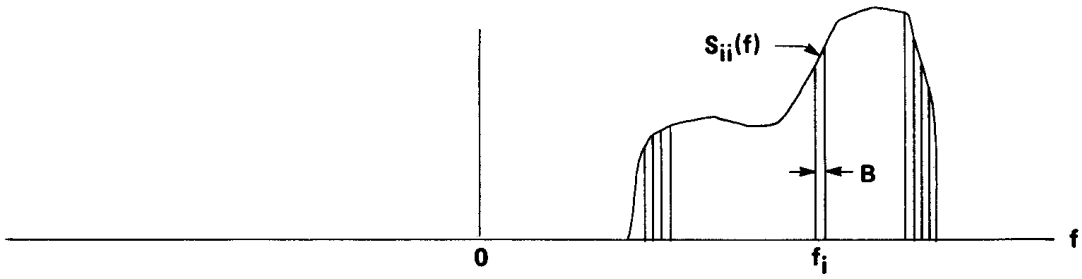

2c. Spectral decomposition of n(t) into W/B uncorrelated components $n_i(t)$ with individual spectra $S_{ii}(f)$.

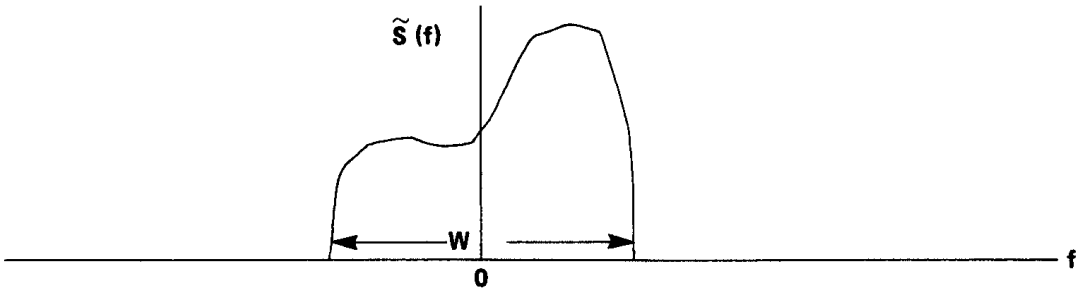

Spectrum of the complex envelope $\tilde{n}(t) = n(t)e^{-j\omega_c t}$

FIGURE 2 Spectral relation of signal, analytic signal, and envelope processes.

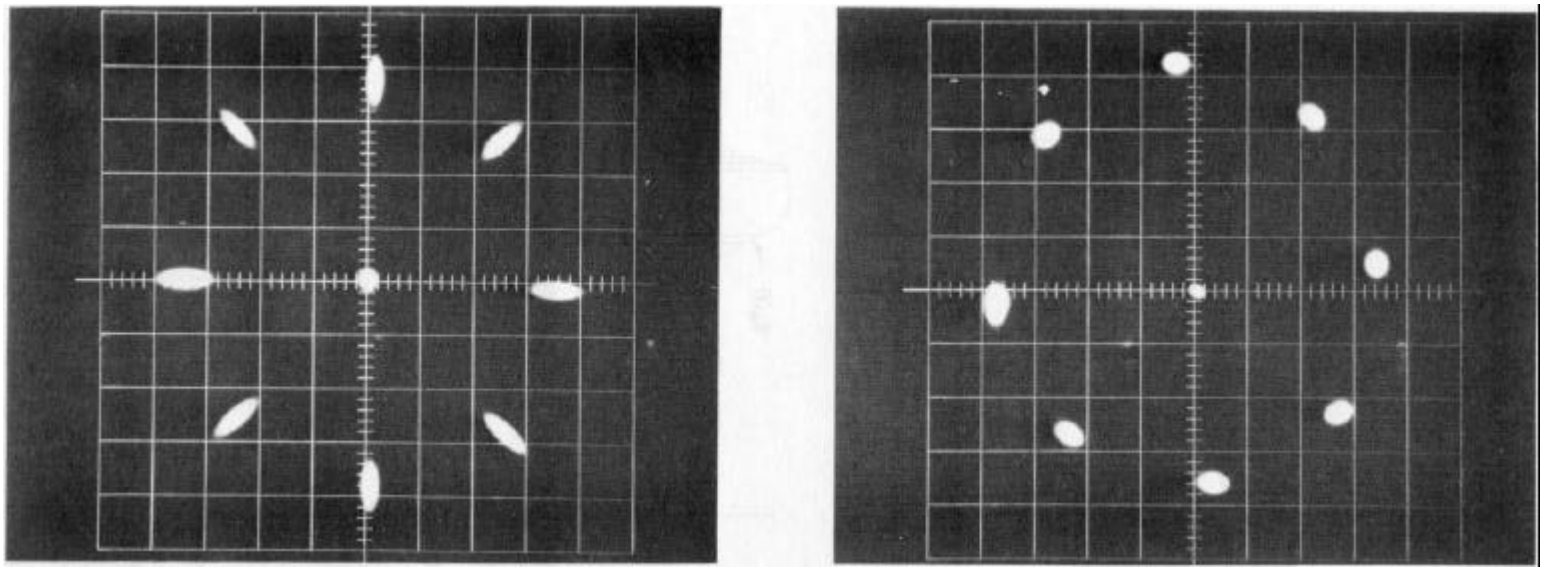

A) P = 3.1 (4.0dB)
B = 20 MHz T = 4.8 nsec
(SINCBT = .985)

B) P = 8.5 (9.3 dB)
B = 20 MHz T = 65 nsec
(SINCBT = –.2)

FIGURE 3 ERROR CONCENTRATION ELLIPSES FOR DFD MEASUREMENTS AT 8 FREQUENCIES, AND WITH NO SIGNAL (CENTRAL ELLIPSE)